A Variable-Volume Optical Pressure–Volume–Temperature Cell for High-Pressure Cloud Points, Densities, and Infrared Spectra, Applicable to Supercritical Fluid Solutions of Polymers up to 2 kbar

Christopher James Gregg,† Fred P. Stein,† Charles K. Morgan,‡ and Maciej Radosz*,‡

Department of Chemical Engineering, Lehigh University, Bethlehem, Pennsylvania 18015, and Exxon Research and Engineering Company, Annandale, New Jersey 08801

A new high-pressure variable-volume optical cell equipped with a sapphire window, a movable piston with a position sensor, and infrared fiber optic probes is described. The apparatus was tested by measuring the cloud points for the system propylene + poly(ethylenepropylene) at 100 and 150 °C, the densities of ethylene and propylene up to 1000 and 600 bar, respectively, and the midinfrared spectra of hexane at 500 bar.

Introduction

The unique properties of supercritical fluids, such as pressure-tuned densities, viscosities, diffusivities, and polarizability, can be exploited in polymerization reactions and polymer fractionation; particle formation, such as the preparation of powders and films (*1*, *2*), fibers (*3*), and particles of controlled size and morphology (*4–8*); and impregnated polymer substrates. These applications require accurate phase equilibrium data and fundamental knowledge of solute–solvent interactions. To obtain such data, we built a variable-volume optical pressure–volume–temperature (PVT) cell for high-pressure measurements of cloud points, densities, and infrared spectra for supercritical mixtures containing polymers. The cell design is the most recent in a series of high-pressure phase behavior probes for supercritical fluid systems and polymers, such as a flow cell for continuous sampling (*9*), recirculating cell for on-line GC sampling (*10*), mass-spectrometer optical cell (*11*), reflect-mode low-angle light scattering (LALS) (*12*), and transmitted LALS (*13*) cells for cloud points in polymer films. These techniques complement existing approaches to equilibrium (*14*, *15*), PVT (*16–19*), and spectroscopy measurements (*20–23*). Our goal is to visually observe the cloud points through a sapphire window, to control the pressure and volume by moving an internal piston (*11–23*), to measure densities using a piston position sensor, and to record the infrared spectra through remote fiber optic probes (*24*, *25*).

Equipment Description

Unit Layout. Although the high-pressure variable-volume optical cell is the hub of the unit, high-pressure tubing, valves, transducer, and pumps support the routine operation of the experiment. A schematic of the apparatus is shown in Figure 1. Upstream of the cell, one high-pressure hand pump (High Pressure Equipment Model 37-5.75-60) and one high-pressure computerized pump (Advanced Pressure Products Model APG-60KMPC) are used to charge the gas solvent and control piston movement, respectively. The pressure supplied by the pumps is measured with pressure transducers (Heise Model 623) which are regularly checked against a dial gauge (Heise Model CM), which in turn is calibrated against a dead weight tester (Ruska Corp. Model 5201-700). The high-pressure manifold also contains a vent and is connected with a vacuum pump. A gas cylinder enclosed in a hot box supplies the supercritical components. Downstream of the cell is a sample trap (ACE Glass Co. Model 5813-23), a graduated sampling device (Ace Glass Co. Model 5758-10), and a wet test meter (Singer Model AL17-1) which allows for determining the amount of gas charged to the system.

In conjunction with the cell, several other pieces of equipment facilitate the experiment. A permanent horseshoe magnet (Permag Corp. Model 5U2B), which is attached to an air-operated motor located directly beneath the cell (not shown), activates the internal stir bar that enhances component mixing. A camera (Burle Model TC252) and a light source (Lenox FLS150) couple the borescope (Lenox Model 15-D-7) to a monitor (Burle Model TC210), which is used for visually observing cloud points. Fiber optic cables (Foster-Miller Inc., Galileo Electro-Optics Corp.) link the infrared optical probes to the FTIR spectrometer (Bomem Model MB-100) and permit spectroscopic measurements.

Cell Design. The high-pressure variable-volume optical cell, shown in Figure 2, consists of a cylindrical body that was bored out and capped by a front and rear gland. The main body was constructed of 316 stainless steel having an outer diameter of 5.514 cm, an overall length of 13.413 cm, and an inner bore diameter of 0.612 cm and length of 6.510 cm. The front gland that seals and supports the window has four parts: a 416 stainless steel nut, heat treated to a Rockwell Hardness of 45; a sapphire window (Insaco Inc.) with dimensions of 1.270 × 1.270 cm and a *c* axis perpendicular to the acting force; a number 010 Viton O-ring; and a brass or stainless steel cap. The rear gland that connects the cell to the high-pressure computerized pump consists of three parts: a 416 stainless steel nut, heat treated to a Rockwell Hardness of 45; a number 013 Viton O-ring; and a 316 stainless steel tube gland, heat treated to a Rockwell Hardness of 45. Two of the three ports machined into the body allow for charging and sampling the cell, as well as measuring the cell pressure, while the third port allows for temperature sensing. The assembly has been hydrostatically tested to 4000 bar and routinely used to 2000 bar.

Within the main bore, a movable piston is used to vary the volume, pressurize the contents, and isolate the contents from the pressurizing fluid. The 316 stainless steel piston is 1.00 cm in length and has a 0.002-cm clearance with the inner bore wall. Two 0.137 × 0.391 cm Viton O-rings create a dynamic seal that prevents the pressurizing fluid from contaminating the sample. By moving the piston, the cell volume can be continuously varied from ~2.0 to ~0.2 cm^3 corresponding to the rear and front gland limits of the piston.

† Lehigh University.
‡ Exxon Research and Engineering Co.

0021-9568/94/1739-0219$04.50/0

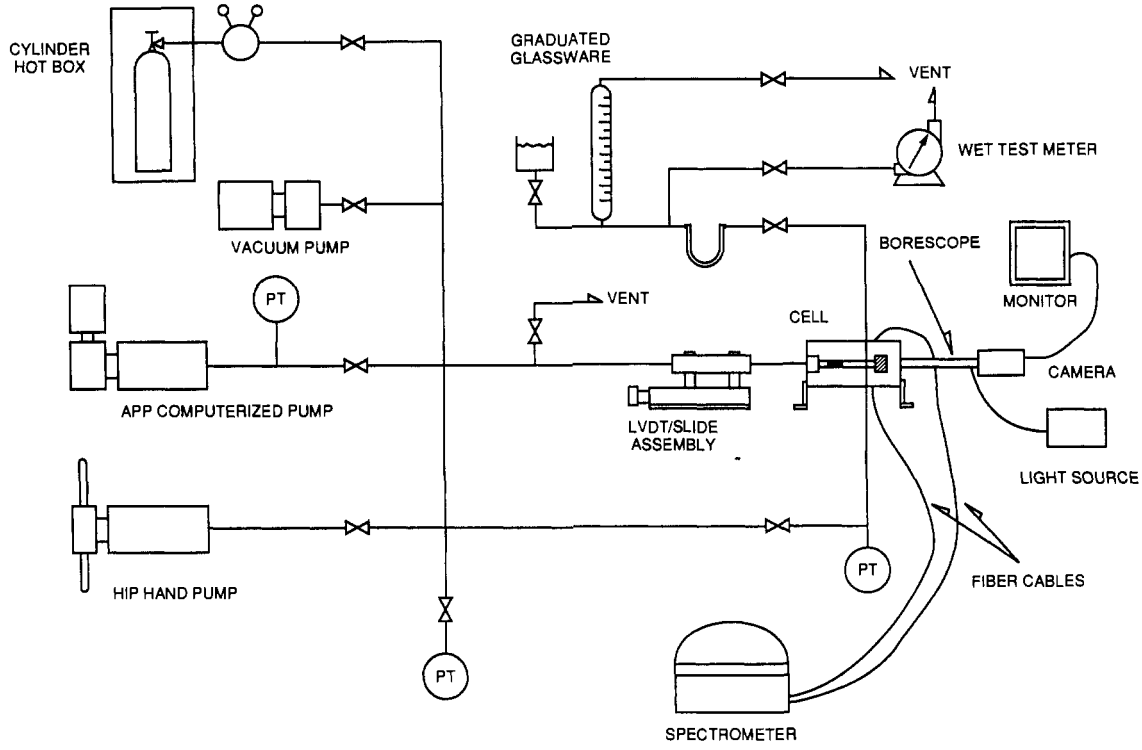

Figure 1. Schematic diagram of the apparatus (PT defined as pressure transducer).

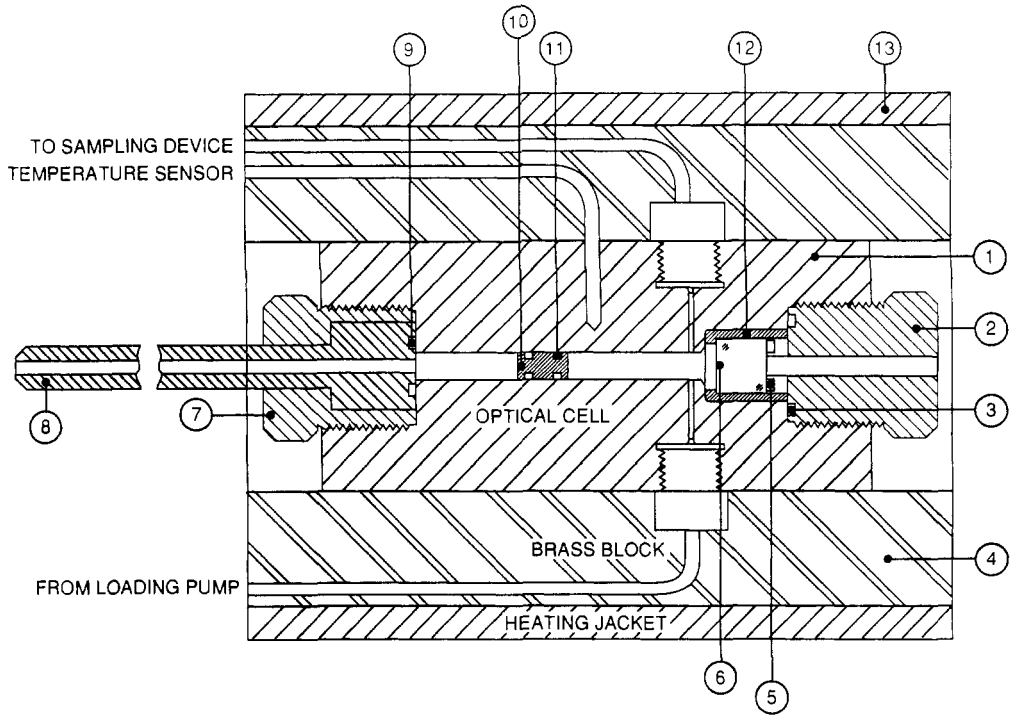

Figure 2. Detailed cell and heating drawing: (1) main body, (2) front gland nut, (3) Viton O-ring, (4) brass heating block, (5) Viton O-ring, (6) sapphire window, (7) rear gland nut, (8) tube gland, (9) Viton O-ring, (10) movable piston, (11) Viton O-ring, (12) brass window cap, (13) heating jacket.

The cell is externally heated using a two-piece 600-W heating jacket (Industrial Heaters Co. Inc. Model A-15894) that fits over the brass block. The heater is wired to a PID controller (Electronic Control Systems Model 6415) which uses a three-wire class A RTD probe (Thermo Electric Co. Inc. Model RTD-18-8-6-LT) as the input sensor. This system allows the inner bore temperature to be controlled to within ±0.05 K; axial and radial temperature gradients were found to be less than ±0.10 K, which set the accuracy of our temperature measurement.

PVT Sensor. The PVT sensor consists of a two-component displacement sensor which tracks the movable piston. As shown in Figure 3, a nonmagnetic 316 stainless steel rod (core-connecting rod) connects the rear of the piston to the core (Lucas Schaveits Model 2790) of a linear variable differential transformer (LVDT). The 316 stainless steel rod and LVDT core are all housed in a nonmagnetic 316 stainless steel tube (long tube gland) that is sealed at the high-pressure computerized pump. The LVDT core position is detected by the second component, the LVDT coil (Lucas Schaveits Model

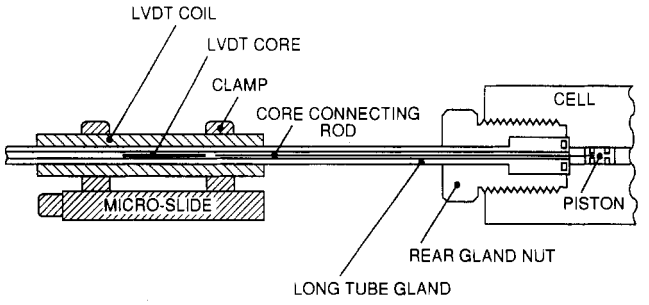

Figure 3. Detailed schematic of the PVT sensor: (1) LVDT core, (2) LVDT coil, (3) microslide, (4) piston–LVDT core–connecting rod.

2000 HR), which fits over the outer diameter of the long tube gland and is clamped on to a high-resolution microslide (Micro Slides Inc. Model 4082-LK, MSA665-8). The core and the coil establish a circuit in which a current can be directly measured using a signal conditioner (Lucas Schaveits Model DTR451) and calibrated to provide a position reading to within ±0.02 mm.

Alternatively, the coil can be moved relative to the core. The microslide can be used to move the coil relative to the core to established the null point (a zero voltage reading in the circuit). This way, the microslide readout (Micro Slide Inc. Model Z515C) measures directly without calibration the distance between two null points to give a piston displacement in the cell. This method is preferred because a higher precision can be attained (±0.002 mm).

Infrared Fiber Optic Probes. In this work two head-to-head probes with bare fiber tips were directly inserted into the bore of the cell. When coupled with a suitable spectrometer and fiber cables, one probe transmits and the other probe receives the IR signal. Figure 4 shows a schematic of the probe orientation looking down the bore of the high-pressure optical cell. The probe body was constructed with a collar that sits within a gland nut which holds the probe in place under pressure and allows variable path lengths from 1 to 50 μm. Number 010 Viton O-rings were used to create a static seal between the probe and cell body.

The 316 stainless steel probe protects the transmitting fiber and houses the fiber sealing mechanism. As shown in Figure 5, the internals consist of a compression nut (Valco Instrument Co. Inc. Model ZN1), polymer ferrule (Valco Instrument Co. Inc. Model FS.4), chalcogenide (Foster-Miller Inc.) or zirconium fluoride (Galileo Elctro-Optics Corp.) fiber, fiber tube aligner (Uniform Tubes Inc.), and a centering bushing (K-Tubes). During assembly, matching surfaces of the probe housing, fiber tube aligner, and centering bushing were coated with epoxy (Epoxy Technology Inc. Model EPO-TEK 353ND) and pressed together. The probe shell was then filled with epoxy, and the fiber inserted through the ferrule. Next, the compression nut was tightened and the assembly heated to set the epoxy thermally. This technique allows the epoxy to hold the fiber stationary and provide a high resistive leak path, while the ferrule creates a hermetic seal. The probes were rigorously tested and found to seal for at least 24 h at pressures in excess of 1500 bar at ambient temperatures. However, at 100 °C the sealing pressure decreased to 1000 bar as the epoxy shear strength decreased from 103 bar (*26*) at 25 °C to 28 bar (*27*) at 200 °C.

Results and Discussion

Cloud Point Measurements: Propylene + Poly(ethylenepropylene). In general, the cloud point experiment consists of loading the cell, equilibrating the system, measuring the cloud points, and then determining the mass of the solvent. First, the cell is loaded by hand with a known mass of polymer, connected to the auxiliary apparatus, and degassed under vacuum. Next, the solvent is added using the high-pressure hand pump. The contents are then pressurized into a one-phase homogeneous solution by advancing the piston while stirring with the magnetically driven stir bar. The system temperature is adjusted, and the contents are allowed to

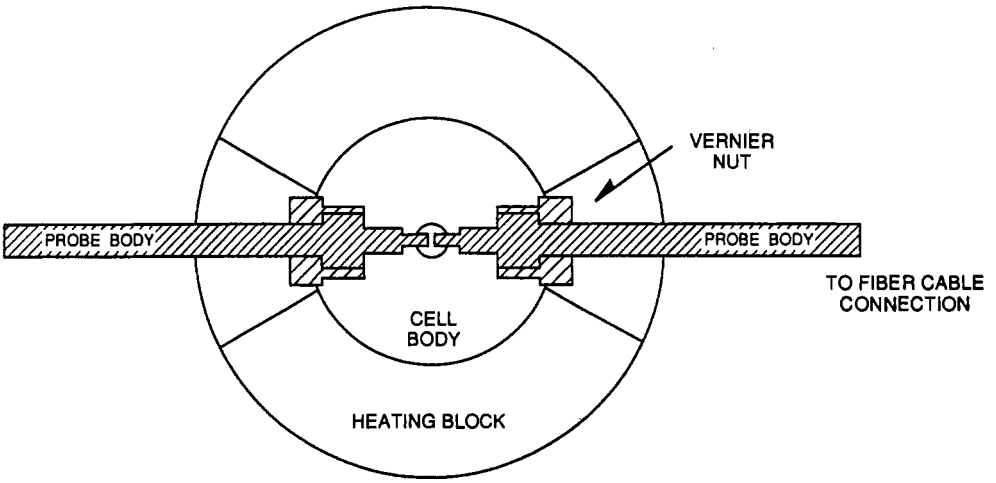

Figure 4. Schematic of the fiber probe orientation looking down the bore of the cell.

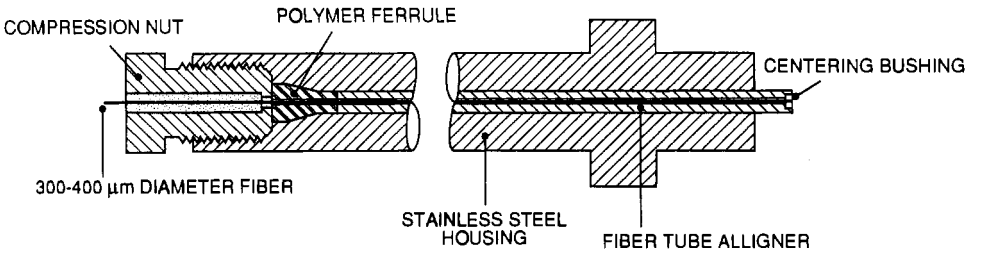

Figure 5. Detailed schematic of the infrared fiber optic probe: (1) compression nut, (2) polymeric ferrule, (3) optical fiber, (4) fiber tube aligner, (5) centering bushing.

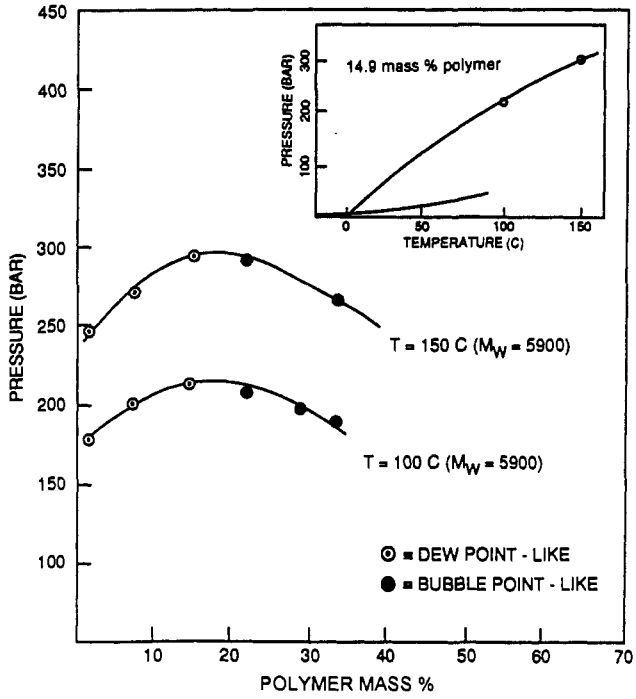

Figure 6. Pressure–concentration cloud point diagram of poly(ethylenepropylene) (PEP, 5900 g/mol) in propylene solutions at 100 and 150 °C. At a given temperature, there is one phase above the curve and two phases below the curve. For comparison, the cloud point curve of Chen and Radosz (28) at 14.9 mass % polymer is plotted in pressure–temperature coordinates (inset) along with the experimental data collected in this work.

equilibrate. Upon equilibration, the sample pressure is lowered by displacing the piston until the clear homogeneous solution, as displayed on the monitor, turns hazy, indicating the onset of immiscibility. At this condition, the pressure is recorded as the cloud point pressure.

At the end of the experiment, the overall sample composition is determined by lowering the cell pressure so that the phases disengage. Then, the volatile component (propylene) is vented to the graduated sampling flask and collected by displacing propylene-saturated water. The volume reading is converted to mass and used with the known mass of loaded polymer to calculate the composition.

The measured cloud point curves in pressure–concentration coordinates for a supercritical propylene solution of monodisperse (28) ($M_w/M_n \leq 1.10$) poly(ethylenepropylene) of molecular weight 5900 g/mol (PEP5.9k) at 100 and 150 °C are shown in Figure 6, and listed in Table 1. These curves represent the miscibility limit of the PEP5.9k in propylene; one phase exists above the curve, and two phases exist below the curve. As shown in Figure 6, the cloud point pressure can be further qualified as dew or bubble point like (28) by visually observing the type of disengagement pattern. This approach allows for estimating the mixture critical point which lies between the dew and bubble point branches of the phase boundary.

For comparison, the cloud point pressures at 14.9 mass % (interpolated) PEP5.9k have been plotted in pressure–temperature coordinates (inset in Figure 6) and are found to be in good agreement with the results of Chen (28) (solid curve).

PVT Measurements*: *Supercritical Ethylene, Subcritical and Supercritical Propylene. At a given pressure and temperature, the density of the fluid is calculated by dividing the mass of the fluid contained within the cell by the volume of the cell. Experimentally, the volume of the cell

Table 1. Experimental Cloud Points for PEP (M = 5900 g/mol) in Propylene

[PEP]/ (mass %)	P/bar (±1.0 bar)	t/°C (±0.1 °C)	transition type[a]
1.8	179.5	100.0	LL(DP)
7.3	202.3	100.0	LL(DP)
15.0	212.5	100.0	LL(DP)
21.6	209.8	100.2	LL(BP)
28.1	200.2	100.3	LL(BP)
32.9	189.1	100.0	LL(BP)
1.8	248.6	150.0	LL(DP)
7.3	273.7	150.0	LL(DP)
15.0	295.0	150.0	LL(DP)
21.6	293.0	150.0	LL(BP)
32.9	267.1	150.0	LL(BP)

[a] Key: LL, liquid–liquid equilibria; BP, bubble point like boundary; DP, dew point like boundary.

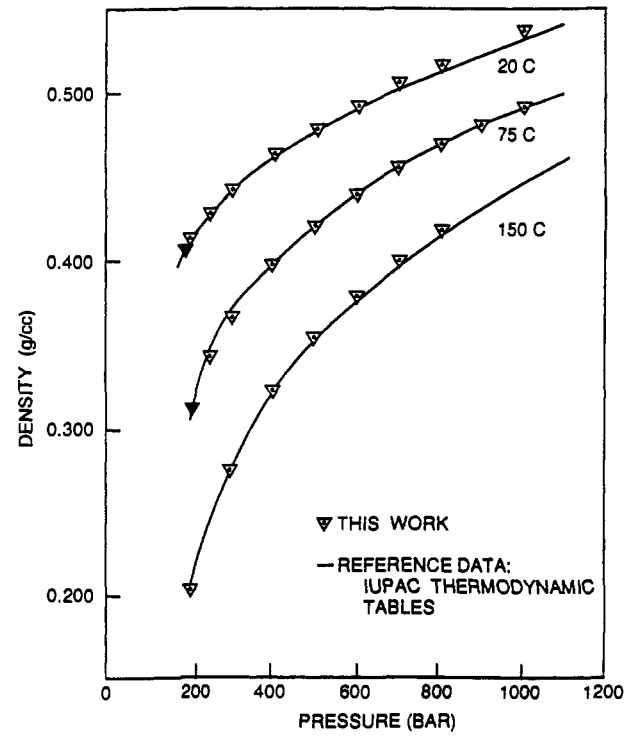

Figure 7. Measured densities for supercritical ethylene at 20.0, 75.0, and 150.0 °C (symbols) compared with the values from the literature (30) (curves).

can be calculated by subtracting the swept piston volume (linear piston displacement multiplied by piston area) from the initial cell volume (piston resting against the tube gland). The initial cell volume was calibrated using argon which has accurately known PVT properties (29). To start an experiment, the fluid of interest is loaded into the cell. With the piston resting on the tube gland, the microslide is moved so that the LVDT is centered over the LVDT core, which establishes the first LVDT null point. At this position, the microslide readout is set equal to zero and all further piston displacements are determined by moving the microslide to locate the new LVDT null point.

Two methods are used to determine the mass of the fluid in the cell, and hence density. If the density is known at any experimental point, as it is for ethylene at 20 °C and 191.1 bar, then the mass can be determined as the product of the known density and the net cell volume at that point. All other densities follow from the measured volume. For example, as shown in Figure 7, the 20 and 75 °C isothermal data sets were determined by fitting the first data point (solid symbol) to the system mass. Alternatively, the ethylene mass can be determined directly by venting it to the graduated

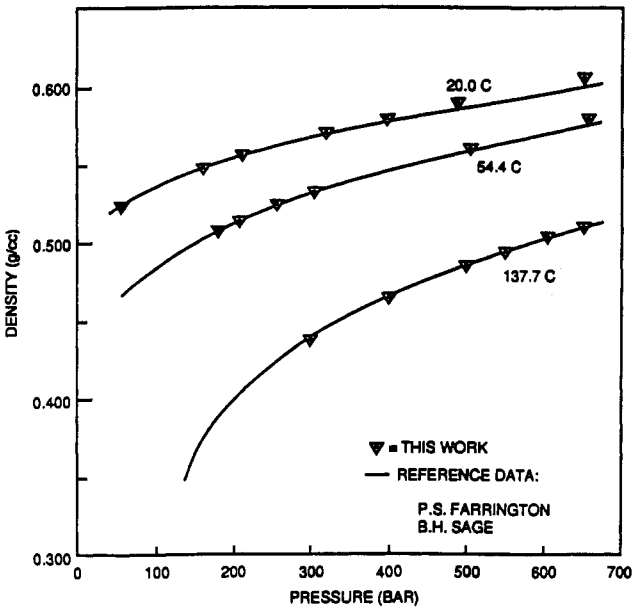

Figure 8. Measured densities for subcritical and supercritical propylene at 20.0, 54.4, and 137.7 °C (symbols) compared with the literature data taken by Farrington and Sage (*21*) (curves).

Table 2. Experimental Densities for Ethylene

t/°C	P/bar	ρ/(g·cm^{-3})	t/°C	P/bar	ρ/(g·cm^{-3})
20.0	191.1	0.4063	75.0	399.9	0.3978
	206.2	0.4125		501.7	0.4221
	258.8	0.4296		600.5	0.4410
	305.2	0.4422		700.3	0.4567
	403.0	0.4629		800.9	0.4708
	501.6	0.4798		900.1	0.4828
	601.7	0.4940		999.4	0.4929
	703.4	0.5066	150.0	203.0	0.2022
	800.6	0.5173		301.1	0.2740
	1001.5	0.5376		402.5	0.3219
75.0	206.3	0.3121		501.4	0.3541
	252.8	0.3424		599.8	0.3798
	302.3	0.3651		702.6	0.4015
				802.0	0.4192

sampling flask and converting the measured volume to mass. The 150 °C isotherm, shown in Figure 7, was determined by this procedure. The agreement between the results obtained in this work and the IUPAC (*30*) values is good for both methods and typically better than 1.0%, the accuracy of our composition measurement. Table 2 lists the experimentally measured densities for ethylene.

To extend the density measurements to less compressible sub- and supercritical fluids, propylene densities were measured at 20.0, 54.4, and 137.7 °C in the range from 50 to 650 bar and are shown in Figure 8. As for ethylene, both methods for determining the fluid mass were employed and shown to be in good agreement with the results of Farrington and Sage (*31*).

These experimental methods were also tested for hysteresis effects. Table 3 lists the measured densities of propylene obtained by increasing and decreasing the pressure; for the 54.4 °C isotherm, no significant hysteresis effect was observed.

Spectroscopic Measurements: High-Pressure Heptane. The spectroscopic measurements consist of selecting suitable transmitting probes, adjusting the sample path length, and then co-adding FTIR scans. The probe type is selected on the basis of what part of the midinfrared region is of interest. As shown by the attenuation curves in Figure 9, the chalcogenide-based fiber probe spans from 3000 to 900 cm^{-1} and the zirconium fluoride-based fiber probe spans from the visible (limited to 6000 cm^{-1} by the spectrometer) to 2000

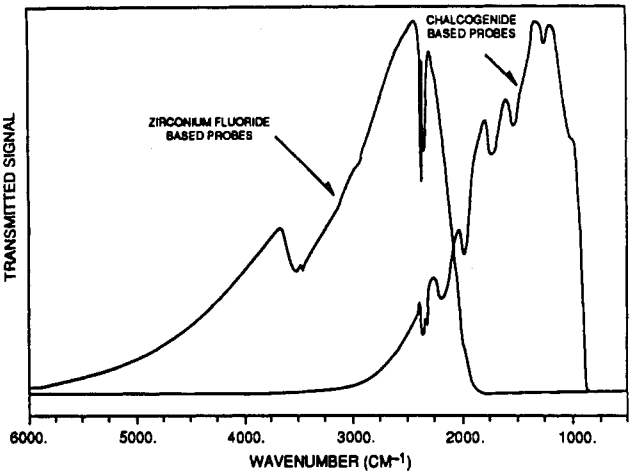

Figure 9. Experimentally measured attenuation curves for the chalcogenide-based fiber probes (2000–1000 cm^{-1}) and the zirconium fluoride-based fiber probes (6000–2000 cm^{-1}). The curves indicate the useful transmitting range of each probe.

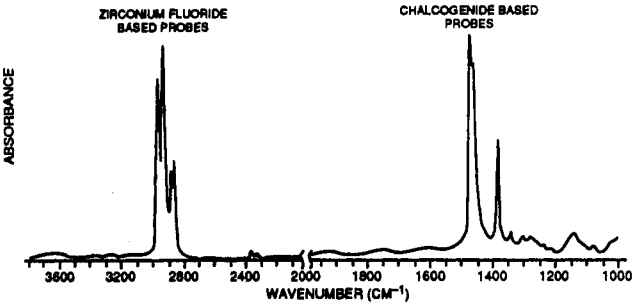

Figure 10. Experimentally measured spectra of heptane at 25 °C and 500 bar using the chalcogenide-based fiber probes (2000–1000 cm^{-1}) and the zirconium fluoride-based fiber probes (3600–2000 cm^{-1}).

Table 3. Experimental Densities for Propylene

t/°C	P/bar	ρ/(g·cm^{-3})	t/°C	P/bar	ρ/(g·cm^{-3})
20.0	54.1	0.5248	54.4	500.7	0.5633
	158.9	0.5479		656.4	0.5811
	210.7	0.5566		304.7	0.5350
	318.9	0.5720		254.5	0.5257
	395.7	0.5809		204.5	0.5150
	647.7	0.6074	137.7	300.1	0.4378
	487.1	0.5919		400.6	0.4654
54.4	179.9	0.5091		499.7	0.4863
	202.3	0.5144		549.6	0.4954
	253.1	0.5252		601.6	0.5039
	304.6	0.5347		650.3	0.5155

cm^{-1}. In order to cover the entire midinfrared region, one has to use both probes independently. Once the probe is selected and connected to the cell, the probe separation (path length) is adjusted to allow for quantitative analysis. Simultaneously, scans are collected and the path length is adjusted by rotating the probe glands until the measured signal falls within the instrument's linearity range, typically less that 1 adsorption unit. Once the path length is fixed, scans are co-added to record the sample spectra.

Figure 10 shows the IR spectra of heptane from 3800 to 1000 cm^{-1} obtained at 25 °C and 500 bar by averaging 192 scans at a wave resolution of 4 cm^{-1}. The measurements were made using a Bomem MB-100 spectrometer with a fiber optic inset, a globar source, and a liquid nitrogen cooled wide band MCT detector. As illustrated in Figure 10, the chalcogenide-based probes are well suited for the C–H bending frequencies between 1380 and 1470 cm^{-1} and the zirconium fluoride-based

probes are well suited for the backbone C–H stretching frequencies in the vicinity of 2940–2855 cm^{-1}.

Conclusions

A new variable-volume optical PVT cell, developed for accurate high-pressure measurements of cloud points, densities, and infrared spectra, has been demonstrated for supercritical fluid solutions of polymers. For example, cloud points for propylene solutions of PEP (M = 5900 g/mol) and ethylene and propylene densities are found to be in good agreement with literature data. Also, the fiber optic probes are demonstrated for remote spectroscopy of heptane at elevated pressures.

Acknowledgment

We are grateful to E. C. Ponce, S. J. Chen, and Professor H. G. Drickamer for critically evaluating our cell design and application. A preliminary account of this work was presented at the Annual Meeting of the American Institute of Chemical Engineers, Los Angeles, CA, 1991 (paper 168B).

Literature Cited

(1) Matson, D. W.; Petersen, R. C.; Smith, R. D. *Mater. Lett.* **1986**, *4* (10), 429–432.
(2) Matson, D. W.; Fulton, J. L.; Petersen, R. C.; Smith, R. D. *Ind. Eng. Chem. Res.* **1987**, *26*, 2298–2306.
(3) Dixon, D. J.; Bodmeiser, R. A.; Johnston, K. P. *AlChE J.* **1993**, *35*, 127.
(4) Mohamed, R. S.; Debenedetti, P. G.; Prud'homme, R. K. *AlChE J.* **1989**, *35* (2), 325–328.
(5) Lele, A. K.; Shine, A. D. *Polym. Prepr.* **1990**, (*Am. Chem. Soc., Div. Polym. Chem.*) *31*, 1.
(6) Lele, A. K.; Shine, A. D. Presented as the 1991 AlChE Annual Meeting, Los Angeles, CA, November 1991.
(7) Tom, J. W.; Debenedetti, P. G. *J. Aerosol Sci.* **1991**, *22* (5), 555–584.
(8) Tom, J. W.; Debenedettii, P. G. *Biotechnol. Prog.* **1991**, *7*, 403–411.
(9) Radosz, M. In *Supercritical Fluid Technology*, Process Technology Proceedings; Penninger, J. M. L., Radosz, M., McHugh, M. S., Krukonis, V. J., Eds.; Elsevier: The Netherlands, 1985; Vol. 3, pp 179–190.
(10) Radosz, M. *Ber. Bunsen-Ges. Phys. Chem.* **1984**, *88*, 859–862.
(11) Chen, S. J.; Randelman, R. E.; Seldomridge, R. L.; Radosz, M. *J. Chem. Eng. Data* **1993**, *38*, 211.
(12) Li, W.; Radosz, M. *Macromolecules* **1993**, *26*, 1417–1423.
(13) Li, W.; Radosz, M. Proceedings of the 204th National Meeting of the American Chemical Society, Washington, DC, 1992.
(14) Dieters, U. K.; Schneider, G. M. *Fluid Phase Equilib.* **1986**, *29*, 149–169.
(15) Alessi, P.; Kikic, I. *Fluid Phase Equilib.* **1990**, *29*, 145–169.
(16) Lesavre, M. M.; Richon, D.; Renon, H. *Ind. Eng. Chem. Fundam.* **1981**, *20*, 254–289.
(17) Holste, J. C.; Hall, K. R.; Eubank, P. T.; Marsh, K. N. *Fluid Phase Equilib.* **1986**, *29*, 161–176.
(18) Dymind, J. H.; Isdale, J. D.; Glen, N. F. *Fluid Phase Equilib.* **1985**, *20*, 305–314.
(19) Sen, Y. L.; Kiran, E. *J. Supercrit. Fluids* **1990**, *3*, 91–99.
(20) Fishman, E.; Drickamer, H. G. *Anal. Chem.* **1956**, *28* (5), 804–806.
(21) Tapavicza, St. v.; Buback, M.; Franck, E. U. *High Temp.—High Pressures* **1976**, *7*, 535–538.
(22) Suppes, G. J.; McHugh, M. A. *Rev. Sci. Instrum.* **1989**, *60* (4), 666–669.
(23) Swaid, I.; Nickel, D.; Schneider, G. M. *Fluid Phase Equilib.* **1985**, *21*, 95–112.
(24) Fitch, P.; Gargus, A. G. *Am. Lab.* **1985**, *17*, 64–71.
(25) Miller, J. F.; Nelson, C. M.; Ludlow, J. M.; Shah, N. N.; Clark, D. S. *Biotechnol. Bioeng.* **1989**, *34*, 1015–1021.
(26) *Handbook of Adhesives Bonding*; Cagle, C. V., Ed.; Lee, H., Neville, K., Cons. Eds.; McGraw-Hill Book Co.: New York, 1972.
(27) Epoxy Technology Inc. technical data sheet for EPO-TEK 353ND.
(28) Chen, S. J.; Radosz, M. *Macromolecules* **1992**, *25*, 3089–3096.
(29) Parrish, W. R. *Fluid Phase Equilib.* **1984**, *18*, 279–297.
(30) *International Thermodynamic Tables of the Fluid State, Ethylene*; Angus, S., Armstrong, B., De Reuk, K. M., Eds.; International Union of Pure and Applied Chemistry; Pergamon Press: New York, Vol. 2.
(31) Farrington, P. S.; Sage, B. H. *Ind. Eng. Chem.* **1949**, *41*, 1734, 1784.

Received for review April 7, 1993. Accepted October 22, 1993.•

• Abstract published in *Advance ACS Abstracts*, December 1, 1993.